RSC Advances

ROYAL SOCIETY OF CHEMISTRY

www.rsc.org/advances

Effect of Silane-Functionalized TiO_2 on the Optical Properties and Moisture Barrier of Silicone Resin Nanocomposites

Wei-Hao Liao, Sheng-Tsung Hsiao, Yi-Fang Wu, Shi-Jun Zeng, Shin-Ming Li, Yu-Sheng Wang and Chen-Chi M. Ma*

Department of Chemical Engineering,

National Tsing-Hua University,

Hsin-Chu 30013, Taiwan

Summited to

RSC Advances

*Corresponding author: Chen-Chi M. Ma

Tel: 886-35713058 Fax: 886-35715408

E-mail: ccma@che.nthu.edu.tw (Chen-Chi M. Ma)

Abstract

This study proposes an effective approach for fabricating silane-functionalized TiO_2 nanoparticles/silicone resin (SR) composites that exhibit high transparency, high refractive indexes (RIs), high UV aging resistance, and high moisture barrier. The surfaces of TiO_2 nanoparticles (TMOS-m-TiO_2) were modified by a sol-gel process using tetramethoxyl (octadecyl) silane (TMOS). The TMOS-m-TiO_2 exhibited a significant improvement in compatibility with the SR matrix. The TMOS-m-TiO_2/SR composite, containing 0.1 phr of TMOS-m-TiO_2, maintained an optical transmittance above 80% in the visible wavelength region. The RI increased with the increasing of TMOS-m-TiO_2 content, and the RI of the 0.10 phr TMOS-m-TiO_2/SR composite was 1.566 (the RI of the neat SR was 1.541). Furthermore, the water vapor transmission rate of 0.10 phr TMOS-m-TiO_2/SR composite was 32.8% lower than that of neat SR. This approach can be applied for developing high-performance SR composite materials that can be used in various applications, particularly in light-emitting (LED) diode encapsulants.

1. Introduction

Light-emitting diodes (LEDs) have received much attention for general lighting applications, such as display backlighting, automotive lighting, and traffic signals, because of their energy efficiency and durability.[1-3] LEDs are expected to replace traditional lighting devices and become the most common lighting source in the next generation. The encapsulant materials for LED packaging play a crucial role in protecting the device from moisture and impact and enhance the extraction of light from the LED chip to air.[4] However, the current LED industry tends to develop high-watt LEDs for wide application, and the traditional LED encapsulant materials are epoxy resins, which do not meet the requirements of high-watt LEDs.[5-7] Because epoxy resins easily undergo heat - and radiation- induced degradation (yellowing) in a high-watt LED operating state, the yellowing epoxy resins cause the lifetime of the device to be short and a critical decline in light output over time.[4, 8] To solve these problems, silicone resins (SRs) have been considered replacement encapsulant materials for current high-watt LED packing because of their satisfactory transparency and excellent UV and thermal resistance.[4, 9-13]

However, SRs exhibit disadvantages, such as a low refractive index (RI) and low resistance to moisture permeability.[14-17] According to Snell's law,[4] an LED encapsulant exhibiting a low RI causes the light emitted from an LED chip (the RI of

an LED chip is between 2.5 and 3.5) to the encapsulant to form a low critical angle at the encapsulant-chip interface, which generates internal reflection on the encapsulant-chip interface, reducing the efficiency of light extraction from the chip to air.[4, 18, 19] Substantial light extraction from the LED chip to the high-RI encapsulant was produced ; therefore, the development of an SR-based LED encapsulant material with a high RI is necessary.[10]

Previous reports[9, 20] have proposed various approaches to increase the RI of polymer materials, such as incorporating aromatic groups into the backbone or side chain of matrices. However, materials with numerous benzene-ring structures tend to crack and yellow under high-temperature conditions, causing the reliability of LED devices to be low. Another methods[21, 22] involved introducing high-RI inorganic nanofillers into polymer matrices. High-RI nanomaterials used to reinforce optical polymeric matrices have generated substantial interest in industry and science, because they can increase the RI of polymeric composites and improve mechanical, thermal, electrical, and moisture barrier properties.[17, 23-25] Several inorganic materials with high RIs are suitable candidates for reinforcing polymeric matrices. The most commonly employed inorganic materials are metal oxides, such as TiO_2, ZrO_2, ZnO_2, SnO_2, CeO_2, and ZnS.[22, 26-29] Among these nanomaterials, TiO_2 is suitable for increasing the RI of optical SRs because of its high RI (between 2.4 and

2.7), low cost, and low absorption coefficient in the visible range.[30-32]

According to Rayleigh's law,[33] if the diameters of nanoparticles larger than 40 nm are more than one-tenth of the minimal wavelength of visible light (400 nm), then the optical scattering phenomenon occurs in the composites. Because nanomaterials with a high specific surface area tend to aggregate easily because of the attractive Van der Waals forces between nanoparticles,[34, 35] the highly aggregated nanomaterial in composites may cause excess optical scattering and reduce the transparency of polymer-based encapsulate materials. Therefore, in order to improve the dispersibility and compatibility of TiO_2 in SR matrices, the development of TiO_2 modification methods is critical.

Although previous studies[36-39] have used functionalized TiO_2 as a nanofiller in various optical polymeric composites, few studies have used functionalized TiO_2 nanofiller as a reinforcement nanomaterial in SR composites. Wang et al.[40] have dispersed the pristine TiO_2 (an average diameter of 21 nm) in SR for encapsulation of GaN-based blue LED, but the aggregated TiO_2 was observed in their SEM result. Liu et al.[41] have modified TiO_2 by organic surfactant, and improved the dispersion of TiO_2 in SR matrix as encapsulant for LED packaging. However, the moisture barrier properties and UV aging of LED encapsulant materials are very important. Few researches study the moisture barrier properties and UV aging of the modified

TiO_2/SR composites.

This study proposes an effective method for inhibiting the aggregation of particles, and improving the compatibility of inorganic particles by using SRs. Tetramethoxyl (octadecyl) silane (TMOS) was employed as a coupling agent to modify TiO_2 (TMOS-m-TiO_2) by using a sol-gel approach, dispersing the TMOS-m-TiO_2 nanoparticles into the SR. Grafting TMOS silane onto the TiO_2 surface provided a good interfacial compatibility with SR matrix to prevent aggregation, and the TMOS-modified TiO_2 with hydrophobic octadecyl molecular chains increased the permeation pathway of the water vapor molecules, enhancing the moisture barrier properties of the SR. Furthermore, the well-dispersed TMOS-m-TiO_2 in the SR maintained a high transmittance of composites beyond the LED optical requirement and improved the UV aging of TMOS-m-TiO_2/SR composites. Moreover, the RI of composites increased as the TMOS-m-TiO_2 content increased, and an RI of 1.566 was achieved (0.10 phr TMOS-m-TiO2/SR composite), suggesting their potential application in LED encapsulant materials.

2. Experimental

2.1 Materials

Tetramethoxyl (octadecyl) silane (TMOS, ≥88%) was received from Aldrich

Chemical Co, St. Louis, MO., USA. TiO_2 was obtained from PlasmaChem GmbH, Krefeld, Berlin, Germany, and the particle size of TiO_2 is 4-8 nm. Tetrahydrofuran (THF, 99.8%), and Hydrochloric Acid (HCl, 36.5%) were received from the Showa Chemical Co., Tokyo, Japan. Silicone resin (OE-6631A and OE-6631B with a weight ratio of 1:2) was obtained from Dow Corning Toray Co. Ltd., Tokyo, Japan.

2.2. Modification of TiO_2

TiO_2 particles were dried under vacuum at 60 ℃ for 24 h before use. Dried TiO_2 particles (60 mg) and HCl (0.01 mol) were added into 100 ml THF by a three-necked flask, and were dispersed at room temperature for 30 min by sonication. TMOS (52 mg) was further added to the solution, and the mixture was stirred with a magnetic stirrer at 60 °C for 2 h under nitrogen atmosphere. Then the flask was put in an ice bath for 1 h to terminate the reaction, and the TMOS-m-TiO_2 nanoparticles dispersed in THF solution were obtained. The TMOS-m-TiO_2/THF solution was centrifuged at 10,000 rpm for 45 min, and then filtered and washed with THF. This process was repeated for five times. The TMOS-m-TiO_2/THF solution was dried at room temperature in vacuum for 24 h. Figure 1 shows the procedure for preparing TMOS-m-TiO_2. Compared with the previous reports[36, 41-43], this study specially selected TMOS to modify TiO_2 particles, since the grafted octadecyl molecular chain

can provide a hydrophobic property on the TMOS-m-TiO_2 surface. This hydrophobic property of TMOS-m-TiO_2 is expected to enhance the interfacial compatibility with the SR matrix and decrease the water vapor transmission rate of the TMOS-m-TiO_2/ SR composites.

2.3 Preparation of the pristine TiO_2/SR and the TMOS-m-TiO_2/SR composites by the solution method

The pristine TiO_2 and TMOS-m-TiO_2 nanoparticles were dispersed in THF (10 ml) respectively, and these TiO_2/THF solutions were mixed homogeneously with OE-6631B (30 g) in a reactor at 25 ℃ for 1h by mechanical stirrer. After the mixture of TiO_2/OE-6631B was dispersed in THF uniformly, the THF solvent was evaporated at 25 ℃ in a vacuum oven for 2h. Then the OE-6631A (60 g) was mixed with the TiO_2/OE-6631B by mechanical stirrer for 30 min. The TiO_2/SR mixture was poured into a mold, followed by vacuum evaporation at 30 ℃ for 2 h to eliminate the entrapped air bubbles and to remove the residual THF solvent. The curing reaction was carried out by heat-treatment at 65 ℃ for 30 min, 100 ℃ for 1 h, and 150 ℃ for 2 h. The pristine TiO_2/SR and the TMOS-m-TiO_2/SR composites containing 0.01, 0.05, 0.10 and 0.15 phr of nanofillers were prepared by the above-mentioned experimental steps. The previous reports[41, 44, 45] usually used toluene as solvent to

disperse the nanofillers in SR matrixes. Differently, this study employed THF as solvent to disperse the TiO2 nanoparticles in SR, since THF possessed a lower boiling temperature than toluene, which was easy to remove the residual solvent after mixing process.

2.4 Characterization

An Ultima IV multipurpose X-ray diffraction (XRD) system (Rigaku Co., Sendagaya, Shibuya-Ku, Tokyo, Japan) was used for the X-ray analysis with Cu-Kα radiation (λ = 1.54051 Å). Step scanning was used with 2θ intervals from 2° to 80° with a residence time of 1 s. Thermogravimetric analyses (TGA) were performed with a Du Pont TGA 2900analyzer from 30 to 800 °C in nitrogen (N_2) at a heating rate of 10 °C min^{-1}. Transmission electron microscope (TEM) observations were conducted using a JEM-2100 microscope (JEOL Limited Co., Tokyo, Japan) with 200 kV. The scanning electron microscope (SEM) used in this work was a Hitachi S-4200 SEM (Hitachi Limited, Tokyo, Japan) with an accelerating voltage of 15 kV. The Ultraviolet–Visible (UV–Vis) transmission spectra were measured by a Varian UV-Vis spectrophotometer (Cary 50, Agilent Co., Santa Clara CA, USA), and the thickness of samples is 2 mm. The RI of the composites was measured at 589nm wavelength by an Abbe refractometer (DR-A1, ATAGO, Tokyo, Japan). UV aging of the composites

was tested by a Spot-Light Source UV Machine with the UV wavelength range between 320~380 nm (UT-300, UniveX Company, Taipei, Taiwan), and the samples were undergone the UV exposure under 19mW/cm^2 for 100hrs. The water vapor transmission rate (WVTR, g/m^2-day) of each sample with the size of 10 cm^2 was measured using a permeation test system (MOCON, Permatran-W3/61, Minnesota, USA) at atmospheric pressure, 40 °C and 100% relative humidity (RH).

3. Results and discussion

3.1 Characterization of TMOS modified TiO_2 nanoparticles

The morphology and size of the nanoparticles were characterized using TEM. Figure 2 (a) shows that the diameter of the pristine TiO_2 was approximately 4-8 nm, which is consistent with the data provided by the manufacturer. The pristine TiO_2 consisted of a zero-dimensional nanostructure with a high specific surface area. The pristine TiO_2 exhibited strong interaction between particles by Van der Waals forces, causing TiO_2 to aggregate. The TMOS-m-TiO_2 (as shown in Figure 2 (b)) showed an apparent coating on the TiO_2 surface that was attributed to the grafted octadecyl molecular chain on the TiO_2 particle surface. The diameter of the TMOS-m-TiO_2 was below 20 nm (as shown in Figure 2 (c)), which confirms with the diametric limitation of nanoparticles according to Rayleigh's law and prevents severe optical scattering.[33]

Furthermore, the grafted trimethyl (octadecyl) silane on the TiO_2 particles was not monolayer grafting, because the grafted trimethyl (octadecyl) silane molecules can also provide hydroxyl functional groups for grafting the other trimethyl (octadecyl) silane molecules. This apparent coating on the surface of the TiO_2 is direct evidence that the octadecyl-functional groups were effectively grafted onto the TiO_2 surface.

In order to analyze the surface modification of TiO_2 further, XPS analysis was used to investigate the elemental composition of the surface of the TiO_2 nanoparticles and to detect the functional groups on the TiO_2 nanoparticles based on the chemical shift observations. Figure 3 shows the XPS survey spectra of the pristine TiO_2 and TMOS-m-TiO_2. The spectrum of the pristine TiO_2 exhibited O1s and Ti2p peaks (Figure 3 (a)). After modifying the TiO_2 nanoparticles with TMOS, the XPS survey spectra of the TMOS-m-TiO_2 indicated an evident decrease in the intensity of the Ti2p peak, and showed the additional peaks of C1s (strong intensity), Si2s, and Si2p peaks, compared with the pristine TiO_2 as shown in Figure 3 (b). Because the surface of the pristine TiO_2 was modified with TMOS by using a sol-gel process, the surface of the TiO_2 was covered with the octadecyl molecular chain of TMOS, which is consistent with the TEM observation (as shown in the TEM images of Figure 2 (c)). The results of the XPS survey confirmed that TiO_2 was modified using a sol-gel process.

To illustrate the accomplishment of the TMOS-modified TiO_2 further, a detailed analysis of the XPS O1s spectra is shown in Figure 4. The XPS O1s spectra of pristine TiO_2 indicated the presence of two peaks located at 530.6 and 532.1 eV, which were attributed to bulk oxide (O^{2-}) and hydroxyl (OH) species. The XPS O1s spectra of the TMOS-m-TiO_2 indicated an additional peak at 532.8 eV, originating from the Ti-O-Si bonds.[46] The presence of Ti-O-Si covalent bonding is in satisfactory agreement with the expected structures of TMOS-m-TiO_2 and indicates that TMOS was grafted to the surface of TiO_2 nanoparticles by using a sol-gel process successfully.

TGA is a useful tool for quantifying organic substances grafted on TiO_2, because the organic substances covalently grafted on the surface of TiO_2 are thermally stripped at temperatures ranging from 200 °C to 500 °C.[34] Figure 5 shows typical TGA thermograms that indicate the weight losses of the pristine TiO_2 and TMOS-m-TiO_2. The pristine TiO_2 exhibited a slight weight loss (approximately 5.1 wt%), which was caused by the thermal decomposition of hydroxyl functional groups (-OH).[36] Compared with the thermal decomposition behavior of the pristine TiO_2, the TMOS-m-TiO_2 exhibited a significantly different weight loss curve. The thermal degradation of the TMOS-m-TiO_2 occurred from 100 °C to 500 °C, which was attributed to the thermal degradation of the grafted octadecyl molecular chain on the

TiO_2 particle surface. The weight loss curve of the TMOS-m-TiO2 exhibited few variations from 500 °C to 800 °C. Therefore, the quantity of the surface-grafted octadecyl molecular chain on the TiO_2 particle surface was estimated by comparing the weight loss of the pristine TiO_2 at a temperature higher than 500 °C. Although the volume of grafted TMOS on the TiO_2 surface is very large (as shown in the TEM image of Figure 2(c)), the density of TMOS (0.821 g/cm^3) is much lower than that of the pristine TiO_2 (4.23 g/cm^3). Therefore, the grafted TMOS did not occupy a high weight ratio in the TMOS-m-TiO_2. Furthermore, this study conjectured that the TMOS-m-TiO2 particles were non-spherical (probably disk-like, as seen in Figure 2(b)) after drying the sample on a TEM grid, thus the true particle size should be smaller despite the apparent particle size ~ 20 nm. Based on the TGA results, the weight fraction of the octadecyl molecular chain of the TMOS-m-TiO_2 was estimated to be 14.8 wt%, which was the quantity of TMOS grafted onto the TiO_2 successfully.

The XRD patterns were analyzed to investigate further evidence of modification. The pristine TiO_2 (as shown in Figure 6 (a)) exhibited multiple sharp diffraction peaks, indicating that the pristine TiO_2 consisted of a highly crystallized structure. The pristine TiO_2 exhibited four major intensity diffraction peaks at 25° (101), 38° (004), 48° (200), and 54° (211). These diffraction peaks were consistent with those reported previously.[36] As the pristine TiO_2 was modified with TMOS, the XRD pattern of the

TMOS-m-TiO_2 (as shown in Figure 6 (b)) exhibited only a broad band at 25°, indicating that the grafting of the octadecylic molecular chains screened the Titania peaks[47, 48]. In summary, based on the results of TEM, XPS, TGA, and XRD analyses, the TiO_2 particles were functionalized by grafting with TMOS successfully. The aforementioned evidence indicates an effective method for preparing TMOS-m-TiO_2 and verifies that TMOS can be grafted on the surface of pristine TiO_2, which is expected to enhance the interfacial compatibility between $TiO_2$and SR for restraining the aggregation of TiO_2 nanoparticles in SR composites.

3.2 Surface Morphology of the Fractured Pristine TiO_2/SR and TMOS-m-TiO_2/SR composites

High-resolution SEM images of the fractured surfaces of the sample (as shown in Figure 7) were used to investigate the dispersibility and compatibility of pristine TiO_2 and TMOS-m-TiO_2 in the SR matrix. Figure 7 (a) shows that the neat SR exhibited a smooth surface. Compared with the SEM image of the neat SR, the SEM images of the pristine TiO_2/SR composites (as shown in Figure 7 (b)–(e)) exhibited heterogeneity, the formation of severe aggregation, and substantial roughness on the fractured surface. These observations indicated that the compatibility between the pristine TiO_2 and the SR matrix was low. The formation of severe aggregation was attributed to the high specific surface area and the strong interaction between

nanoparticles through Van der Waals forces of the pristine TiO_2. Compared with the pristine TiO_2/SR composites, the SEM images of the TMOS-m-TiO_2/SR composites (as shown in Figure 7 (f)–(i)) exhibited better dispersions of TMOS-m-TiO_2, and indicated no obvious agglomerates occurred when the TMOS-m-TiO_2 content was below 0.10 phr. Furthermore, the TMOS-m-TiO_2/SR composites with a TMOS-m-TiO_2 content of 0.15 phr exhibited slight aggregation in the small region, suggesting that the TMOS-m-TiO_2 possesses excellent compatibility and dispersibility in the SR matrix. The pristine TiO_2 nanoparticles are easily aggregated due to their high surface energy, and the surface modification of TiO_2 nanoparticles may reduce the TiO_2 surface energy[43]. Therefore, the phenomena of aggregated TiO_2 nanoparticles can be improve by grafting the octadecyl molecular chain on the TiO_2 particle surface. Furthermore, the surface of pristine TiO_2 was hydrophilic. After the surface modification of TiO_2, the surface of TMOS-m-TiO_2 was changed to hydrophobicity, due to the grafted octadecyl molecular chain. The main structure of SR matrix (-Si-O-Si-) and the surface of TMOS-m-TiO_2 were both hydrophobic, thus the grafted octadecyl molecular chain on the TiO_2 surface provided a good interfacial compatibility with SR for effectively inhibiting the aggregation of TiO_2, promoting the dispersibility of TMOS-m-TiO_2 nanoparticles in the SR matrix.

3.3 Optical properties of pristine TiO_2/SR and TMOS-m-TiO_2/SR composites

LED industries require that LED encapsulant materials have a thickness of 2 mm, which enables LEDs to yield optical transmittance greater than 80% at the 450-nm wavelength[4]; thus, maintaining the high optical transmittance of composites is crucial. Figure 8 shows the optical transmittance of the pristine TiO_2/SR and TMOS-m-TiO2/SR composites consisting of various TiO_2 contents. The neat SR exhibited a high transmittance of 94.06% at the 450-nm wavelength. As the pristine TiO_2 content increased from 0 to 0.01 phr (as shown in Figure 8 (a)), the optical transmittance of the pristine TiO_2/SR composite decreased to 79.39%, which is lower than the requirement for LED encapsulant materials. Furthermore, the increase in pristine TiO_2 content in the SR matrix caused a critical decrease in optical transmittance. These results were consistent with those of the SEM observation that indicated that the severe aggregation of pristine TiO_2 in the SR matrix caused light scattering,[33] and the optical transmittance of pristine TiO_2/SR composites evidently decreased. Figure 8 (b) shows the optical transmittance of the TMOS-m-TiO_2/SR composites. As the TMOS-m-TiO_2 content increased from 0 to 0.10 phr, the 0.10-phr TMOS-m-TiO_2/SR composite still exhibited a high optical transmittance of 82.38% at the 450-nm wavelength. These results were consistent with those of the SEM observation and were attributed to the well-dispersed TMOS-m-TiO_2 in the SR matrix.

However, when the TMOS-m-TiO_2 content increased to 0.15 phr, the optical transmittance decreased to 78.21%, which is lower than the requirement for LED encapsulant materials. Compared with the pristine TiO_2/SR composites, the TMOS-m-TiO_2/SR composites exhibit higher optical transmittance. This improvement can be attributed to the homogeneous dispersion of TMOS-m-TiO_2 in the SR matrix, which effectively inhibits light scattering and enables a high optical transmittance can be maintained.

3.4 Optical properties of theTMOS-m-TiO_2/SR composite after UV aging

Most optical polymers undergo yellowing when the polymeric matrix is subjected to UV radiation. This yellowing phenomenon is attributed to the aromatic group or free radicals in optical polymers and reduces optical transmittance. In this study, a thermal aging test was conducted on the SR composites with an optical transmittance greater than 80% at the 450-nm wavelength before UV aging (the SR composite with a TMOS-m-TiO2 content less than 0.10 phr), and the optical transmittance of the SR composites were measured after UV aging. The results are summarized in Table 1 and Figure 9. The neat SR exhibited an optical transmittance of approximately 89.69% after UV aging and a 4.37% transmittance loss compared with the neat SR before UV

aging. The transmittance loss of the TMOS-m-TiO2/SR composite after UV aging decreased as the TMOS-m-TiO_2 content increased in the SR matrix. Increasing the TMOS-m-TiO_2 content to 0.10 phr in the SR composite yielded an only 1.41% transmittance loss after UV aging and enabled an optical transmittance of approximately 80.97% (higher than the applied standard for LED encapsulants) to be maintained. These observations were attributed to the incorporation of UV-absorbing and well-dispersed TMOS-m-TiO_2 in the SR matrix, which increased the UV-light shielding efficiency of the TMOS-m-TiO2/SR composite.

3.5 RI of theTiO_2/SR composite.

In order to increase the efficiency of light extraction from the LED chip to air, TMOS-m-TiO_2 can be used as an RI reinforcement material in SR composites for LED packaging. Figure 10 shows the RI of TiO_2/SR composites with various TiO_2 contents. The RI of the neat SR was approximately 1.541. The RI values of the SR composites increased steadily as the TMOS-m-TiO_2 content increased, and an RI of approximately 1.576 was attained for a TMOS-m-TiO_2 content of 0.15 phr. Compared with the TMOS-m-TiO_2/SR composite, similar trend and RI values were found for the pristine TiO_2/SR composite. Compared to pristine TiO_2/SR nanocomposites at the equal nanofiller content, the large shell region (tetramethoxyl (octadecyl) silane) will decrease the maximum titania loading significantly in the composite indeed. Although

the pure TIO_2 composition content of TMOS-m-TiO_2/SR composite was lower than that of pristine TiO_2/SR composites, the RI of well-dispersed TMOS-m-TiO_2/SR was comparable to that of the aggregated pristine TiO_2/SR. Because the increased RI of composite was caused by refracting the incident light on the TiO_2 surface area, the well-dispersed TMOS-m-TiO_2 particles with high surface area can refract the incident light efficiently. These results indicated that incorporating TMOS-m-TiO_2 into the SR matrix can effectively improve the RI of SR composites.

3.6 The moisture barrier property of theTiO_2/SR composites

To prevent the LED chip from damage caused by dampness, the LED encapsulant materials must exhibit a high moisture barrier to protect the LED chip. The WVTR of the TMOS-m-TiO_2/SR composite was investigated. The results are shown in Figure 11. The WVTR of the TMOS-m-TiO2/SR composites decreased as the TMOS-m-TiO_2 content increased. As the pristine TiO_2 content in the composite increased from 0 to 0.15 phr, the WVTR of pristine TiO_2/SR composite decreased from 20.1 $g/m^2 \cdot day$ to 13.8 $g/m^2 \cdot day$ (approximately decreased 31.3 % compared to neat SR). Compared to the WVTR of pristine TiO2/SR composite, the WVTR of TMOS-m-TiO_2 /SR composite exhibited dramatically decrease with the increasing of the TMOS-m-TiO_2 content. The WVTR of TMOS-m-TiO_2/SR composite containing

0.15 phr TMOS-m-TiO_2 decreased to 8.7 g/m^2·day (approximately decreased 56.7% compared to neat SR). The more effective decrease in WVTR occurred because of the presence of TMOS-m-TiO_2, which was grafted with a hydrophobic octadecyl molecular chain on the TiO_2 surface. Furthermore, incorporating TMOS-m-TiO_2 into the SR matrix increased the tortuous permeation pathway of the water vapor molecules, consequently enhancing the moisture barrier properties of the SR composites.

4. Conclusions

This study proposes an effective approach in which a sol-gel procedure is used to modify the surface of TiO_2 nanoparticles, which exhibited excellent dispersibility and compatibility with the SR matrix. Incorporating well-dispersed TMOS-m-TiO_2 into the SR matrix enabled a high optical transmittance to be maintained and enhanced the RI value, UV aging resistance, and moisture barrier property of the TMOS-m-TiO2/SR composite. The optical transmittance of the TMOS-m-TiO_2/SR composite with 0.10 phr of TMOS-m-TiO_2 maintained approximately 82.38% transparency at the 450-nm wavelength, increasing the RI to 1.566. Based on the results of the literature[40, 41], few reports investigated the moisture barrier properties and UV aging of the TiO_2/SR composites as encapsulant for LED packaging. In this

study, the transmittance loss of the TMOS-m-TiO_2/SR composite after UV aging decreased as the TMOS-m-TiO_2 content increased in the SR matrix. In addition, the moisture barrier property of the TMOS-m-TiO_2/SR composite with 0.10 phr of TMOS-m-TiO_2 decreased by approximately 32.8%, compared with the neat SR. Consequently, the TMOS-m-TiO_2/SR composite provided an effective method for developing SR-based materials featuring high optical performance that can be used in various applications.

Acknowledgment

This work was supported by the Ministry of Science and Technology, Taipei, Taiwan, under Contract No. 103-2221-E-007-001-(103), and NSC 103-2221-E-007-130-(103).

References

1. L. Yeong-Her, Y. Jiun Pyng, L. Yuan-Chang, N. T. Tran and F. G. Shi, *Components and Packaging Technologies, IEEE Transactions on*, 2010, **33**, 761-766.
2. J. S. Kim, S. C. Yang, S. Y. Kwak, Y. Choi, K. W. Paik and B. S. Bae, *J Mater Chem*, 2012, **22**, 7954-7960.
3. Y. Yang, Y. Q. Li, S. Y. Fu and H. M. Xiao, *J Phys Chem C*, 2008, **112**, 10553-10558.
4. L. Yeong-Her, Y. Jiun-Pyng, L. Yuan-Chang, N. T. Tran and F. G. Shi, *Components and Packaging Technologies, IEEE Transactions on*, 2010, **33**, 761-766.

5. N. Gao, W. Liu, S. Ma, C. Tang and Z. Yan, *J Polym Res*, 2012, **19**.
6. N. T. Yan Zhou, Yuan-Chang Lin, Yongzhi He, and Frank G. Shi, *Ieee T Adv Packaging*, 2008, **31**, 484-489.
7. R. Karlicek, Conference on Lasers and Electro-Optics/Quantum Electronics and Laser Science and Photonic Applications Systems Technologies, Baltimore, Maryland, 2005.
8. S. N. Yahya, C. K. Lin, M. R. Ramli, M. Jaafar and Z. Ahmad, *Mater Design*, 2013, **47**, 416-423.
9. S. Yang, J. S. Kim, J. H. Jin, S. Y. Kwak and B. S. Bae, *J Appl Polym Sci*, 2010, **117**, 2140-2145.
10. J.-S. Kim, S. Yang and B.-S. Bae, *Chem. Mater.*, 2010, **22**, 3549-3555.
11. B. S. Bae, J. S. Kim and S. Yang, *J Sol-Gel Sci Techn*, 2010, **53**, 434-440.
12. E. Vanlathem, A. W. Norris, M. Bahadur, J. DeGroot and M. Yoshitake, *Organic Optoelectronics and Photonics II*, 2006, **6192**, 19202-19202.
13. M. Bahadur, A. W. Norris, A. Zarisfi, J. S. Alger and C. C. Windiate, *Proc Spie*, 2006, **6337**.
14. X. Yuan, X. Li, E. Zhu, J. Hu, S. Cao and W. Sheng, *Carbohydr. Polym.*, 2010, **79**, 373-379.
15. N. Gao, W. Liu, Z. Yan and Z. Wang, *Opt Mater*, 2013, **35**, 567-575.
16. H. Chuanxin, Z. Wentao, G. Xue, Z. Haijuan, G. Dayong and L. Jianhong, Electronic Packaging Technology and High Density Packaging (ICEPT-HDP), 2012 13th International Conference on, 2012.
17. Y. He, J. A. Wang, C. L. Pei, J. Z. Song, D. Zhu and J. Chen, *J Nanopart Res*, 2010, **12**, 3019-3024.
18. A. Borbely and S. G. Johnson, Third International Conference on Solid State Lighting, 2004, 5187, 301-308.
19. Y. K. Ee, P. Kumnorkaew, R. A. Arif, H. Tong, Z. Hongping, J. F. Gilchrist and N. Tansu, *Selected Topics in Quantum Electronics, IEEE Journal of*, 2009, **15**, 1218-1225.
20. S. Yang, J. S. Kim, J. Jin, S. Y. Kwak and B. S. Bae, *J Appl Polym Sci*, 2011, **122**, 2478-2485.
21. W.-C. Chen, S.-J. Lee, L.-H. Lee and J.-L. Lin, *J Mater Chem*, 1999, **9**, 2999-3003.

22. P. Tao, Y. Li, A. Rungta, A. Viswanath, J. N. Gao, B. C. Benicewicz, R. W. Siegel and L. S. Schadler, *J Mater Chem*, 2011, **21**, 18623-18629.
23. H. P. Xiang, J. F. Ge, S. H. Cheng, H. M. Han and S. W. Cui, *J Sol-Gel Sci Techn*, 2011, **59**, 635-639.
24. Y. Liu, C. Lü, M. Li, L. Zhang and B. Yang, *Colloids Surf. Physicochem. Eng. Aspects*, 2008, **328**, 67-72.
25. K. W. Lem, D. H. Nguyen, H. N. Kim and D. S. Lee, *J Nanosci Nanotechno*, 2011, **11**, 7202-7205.
26. D. H. Nguyen, H. N. Kim and D. S. Lee, *J Nanosci Nanotechno*, 2012, **12**, 4207-4210.
27. C. L. Yuanrong Cheng, Bai Yang, *Recent Patents on Materials Science*, 2010, **4**, 15-27.
28. Z. Yuan, W. Zhou, T. Hu, Y. Chen, F. A. N. Li, Z. Xu and X. Wang, *Surface Review and Letters*, 2011, **18**, 33-38.
29. L. Yan, L. Ziyin, Z. Xueying, Y. Sehoon, M. Kyoung-sik and C. P. Wong, Electronic Components and Technology Conference (ECTC), 2012 IEEE 62nd, 2012.
30. N. Nakayama and T. Hayashi, *J Appl Polym Sci*, 2007, **105**, 3662-3672.
31. W. C. Chen, S. J. Lee, L. H. Lee and J. L. Lin, *J Mater Chem*, 1999, **9**, 2999-3003.
32. C. L. Lu and B. Yang, *J Mater Chem*, 2009, **19**, 2884-2901.
33. H. Althues, J. Henle and S. Kaskel, *Chem. Soc. Rev.*, 2007, **36**, 1454-1465.
34. W.-H. Liao, S.-Y. Yang, J.-Y. Wang, H.-W. Tien, S.-T. Hsiao, Y.-S. Wang, S.-M. Li, C.-C. M. Ma and Y.-F. Wu, *ACS Appl Mater Interfaces*, 2013, **5**, 869-877.
35. W.-H. Liao, H.-W. Tien, S.-T. Hsiao, S.-M. Li, Y.-S. Wang, Y.-L. Huang, S.-Y. Yang, C.-C. M. Ma and Y.-F. Wu, *ACS Appl Mater Interfaces*, 2013, **5**, 3975-3982.
36. P. Tao, Y. Li, A. Rungta, A. Viswanath, J. Gao, B. C. Benicewicz, R. W. Siegel and L. S. Schadler, *J. Mater. Chem.*, 2011, **21**, 18623-18629.
37. M. Yoshida, M. Lal, N. D. Kumar and P. N. Prasad, *Journal of Materials Science*, 1997, **32**, 4047-4051.
38. M. Yoshida and P. N. Prasad, *Chem. Mater.*, 1996, **8**, 235-241.
39. S. A. Carter, J. C. Scott and P. J. Brock, *Applied Physics Letters*,

1997, **71**, 1145-1147.
40. P.-C. Wang, C.-L. Lin, Y.-K. Su, P.-C. Chien, Y.-H. Yeh, J.-K. Liou and C.-M. Wei, *JaJAP*, 2014, **53**, 06JE10.
41. L. Yan, L. Ziyin, Z. Xueying, M. Kyoung-sik, Y. Sehoon, J. Choi and C. P. Wong, Electronic Components and Technology Conference (ECTC), 2013 IEEE 63rd, 2013.
42. D. H. Nguyen, H. N. Kim and D. S. Lee, *Journal of Nanoscience and Nanotechnology*, 2012, **12**, 4207-4210.
43. H. Xia and Q. Wang, *Chem. Mater.*, 2002, **14**, 2158-2165.
44. G.-W. Lee, J. Lee, S.-S. Lee, M. Park and J. Kim, *Journal of Materials Science*, 2005, **40**, 1259-1263.
45. Z. Li, W. Lin, K.-S. Moon, S. J. Wilkins, Y. Yao, K. Watkins, L. Morato and C. Wong, *Carbon*, 2011, **49**, 4138-4148.
46. B. Erdem, R. A. Hunsicker, G. W. Simmons, E. D. Sudol, V. L. Dimonie and M. S. El-Aasser, *Langmuir*, 2001, **17**, 2664-2669.
47. C. Mao, H. Li, F. Cui, Q. Feng, H. Wang and C. Ma, *J. Mater. Chem.*, 1998, **8**, 2795-2801.
48. K. V. P. M. Shafi, A. Ulman, X. Yan, N.-L. Yang, M. Himmelhaus and M. Grunze, *Langmuir*, 2001, **17**, 1726-1730.

LIST OF FIGURES

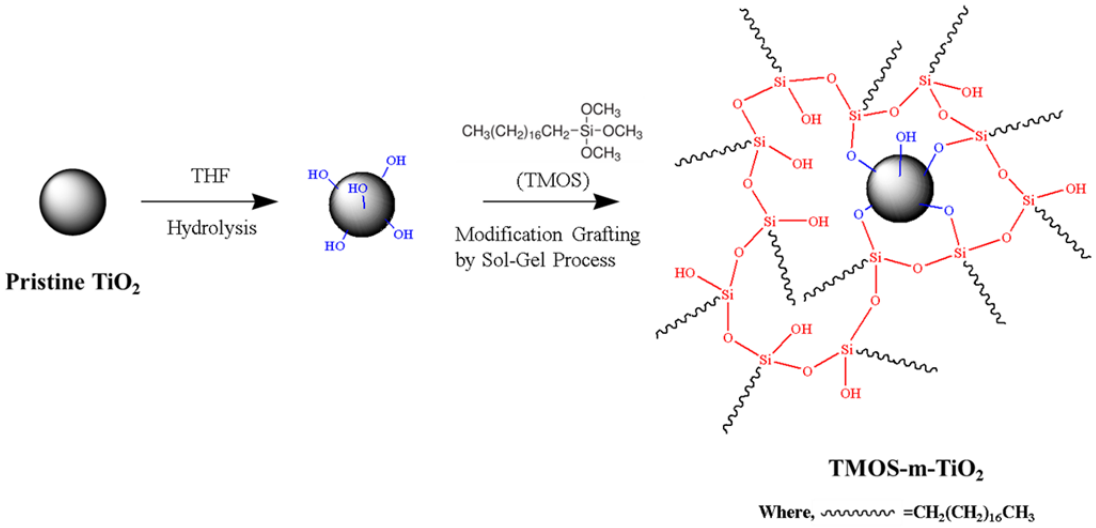

Figure 1. Scheme of the procedure for preparation of TMOS-m-TiO_2.

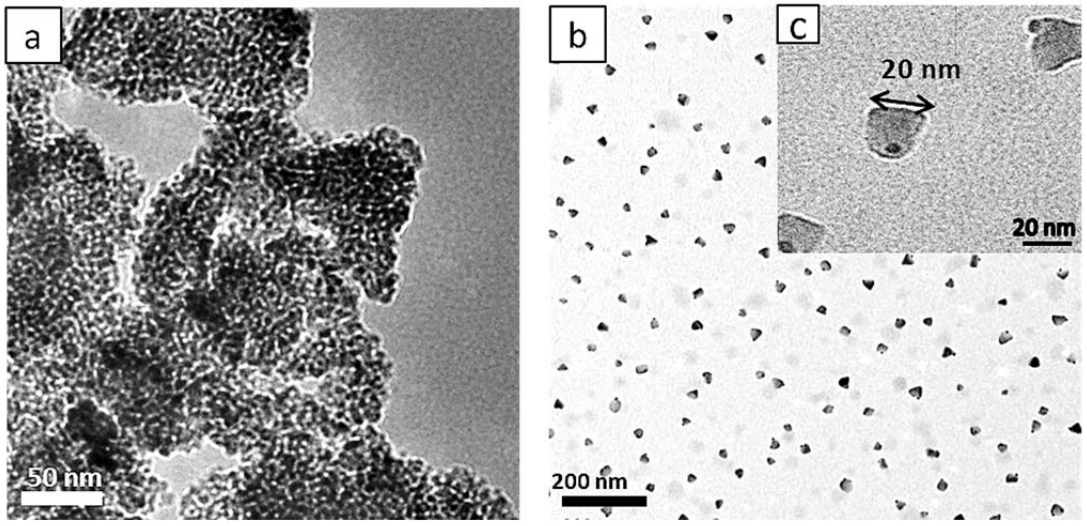

Figure 2. TEM image of nanoparticles: (a) pristine TiO_2, (b) and (c) TMOS-m-TiO_2.

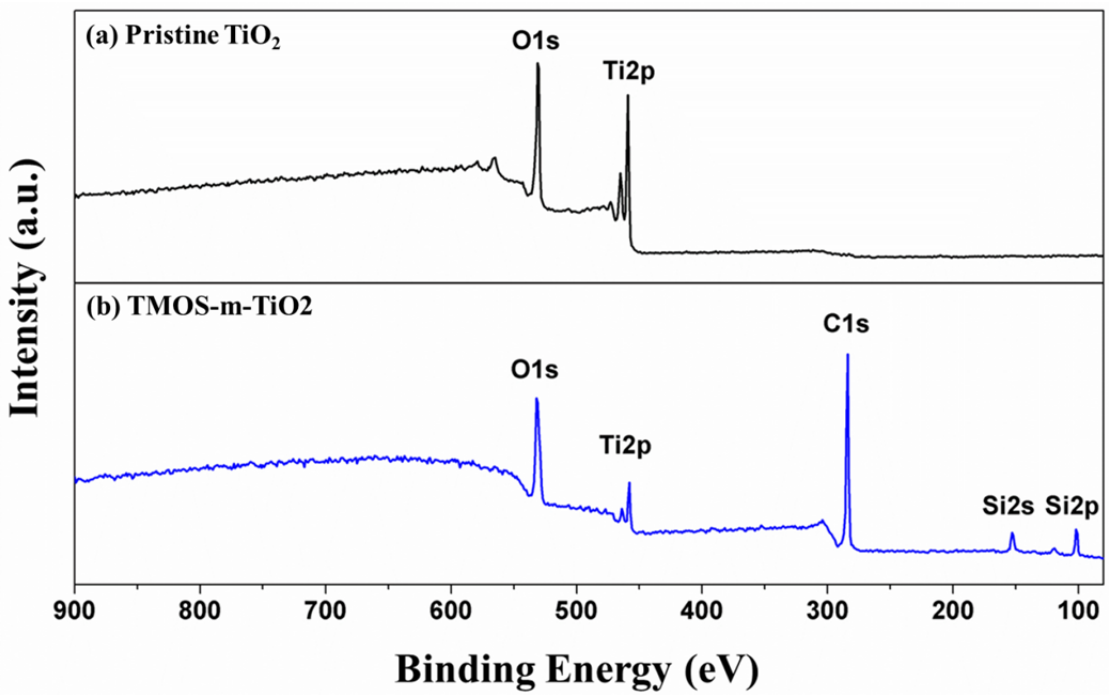

Figure 3. XPS survey scans of (a)pristine-TiO_2, (b)TMOS-m-TiO_2.

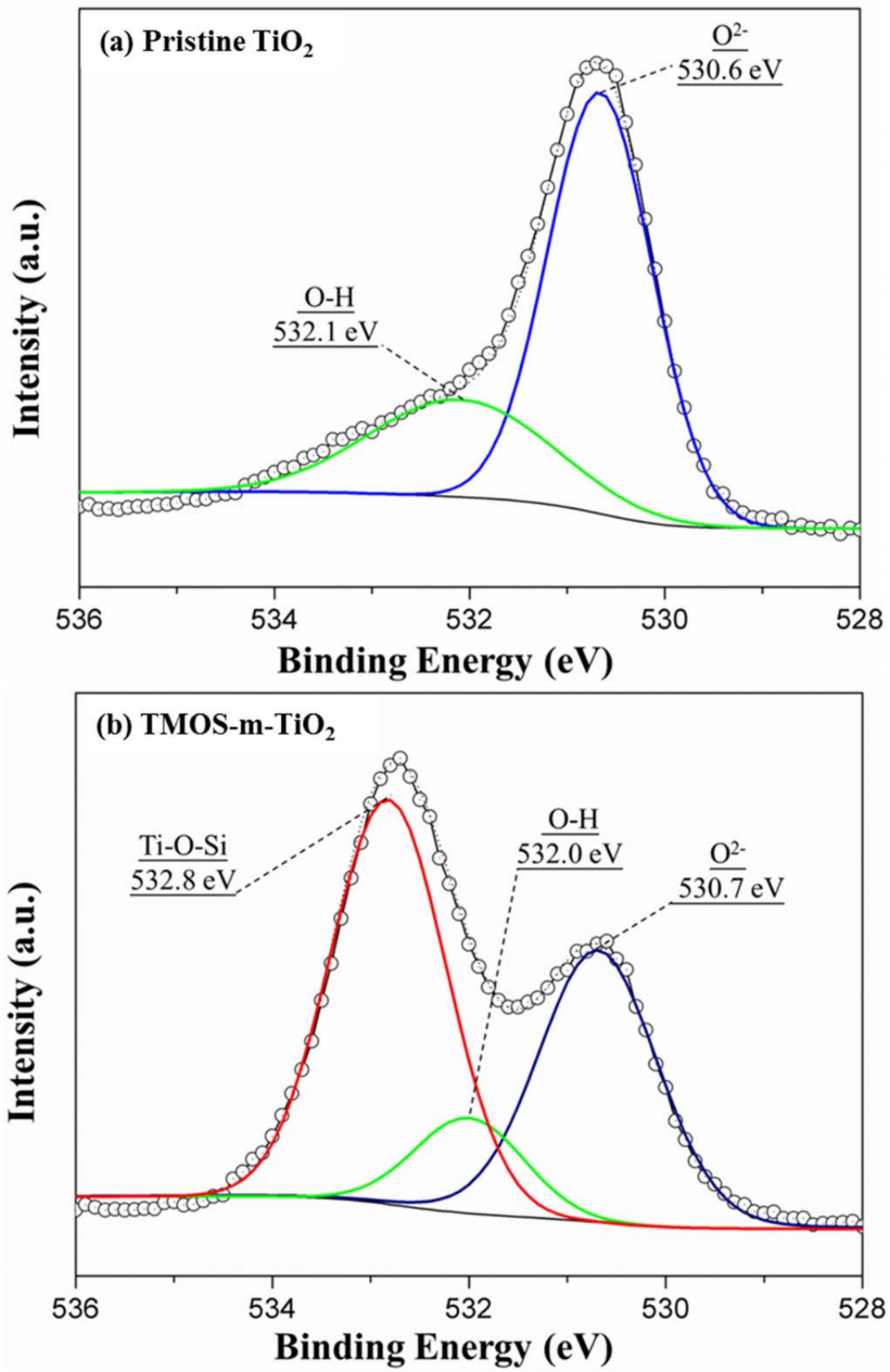

Figure 4. High resolution O1s XPS spectra of (a) pristine TiO_2, (b)TMOS-m- TiO_2.

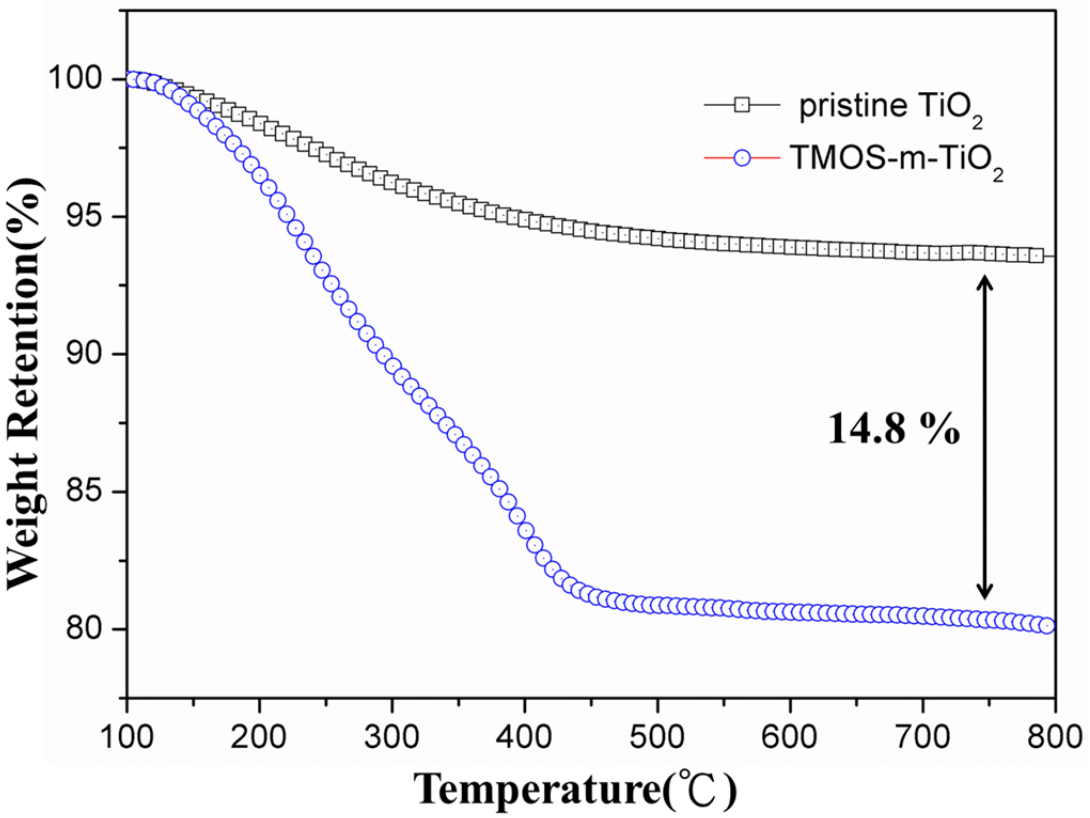

Figure 5. TGA curves of pristine TiO_2 and TMOS-m-TiO_2.

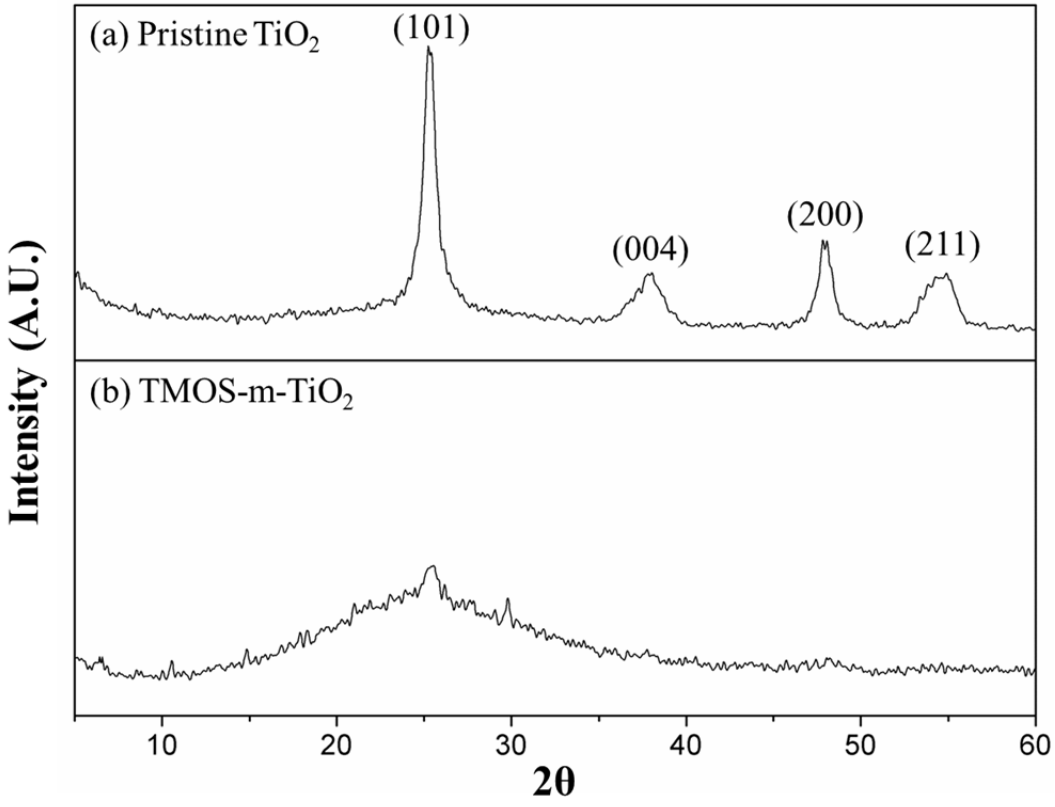

Figure 6. XRD patterns of nanoparticles: (a) pristine-TiO_2, (b) TMOS-m-TiO_2.

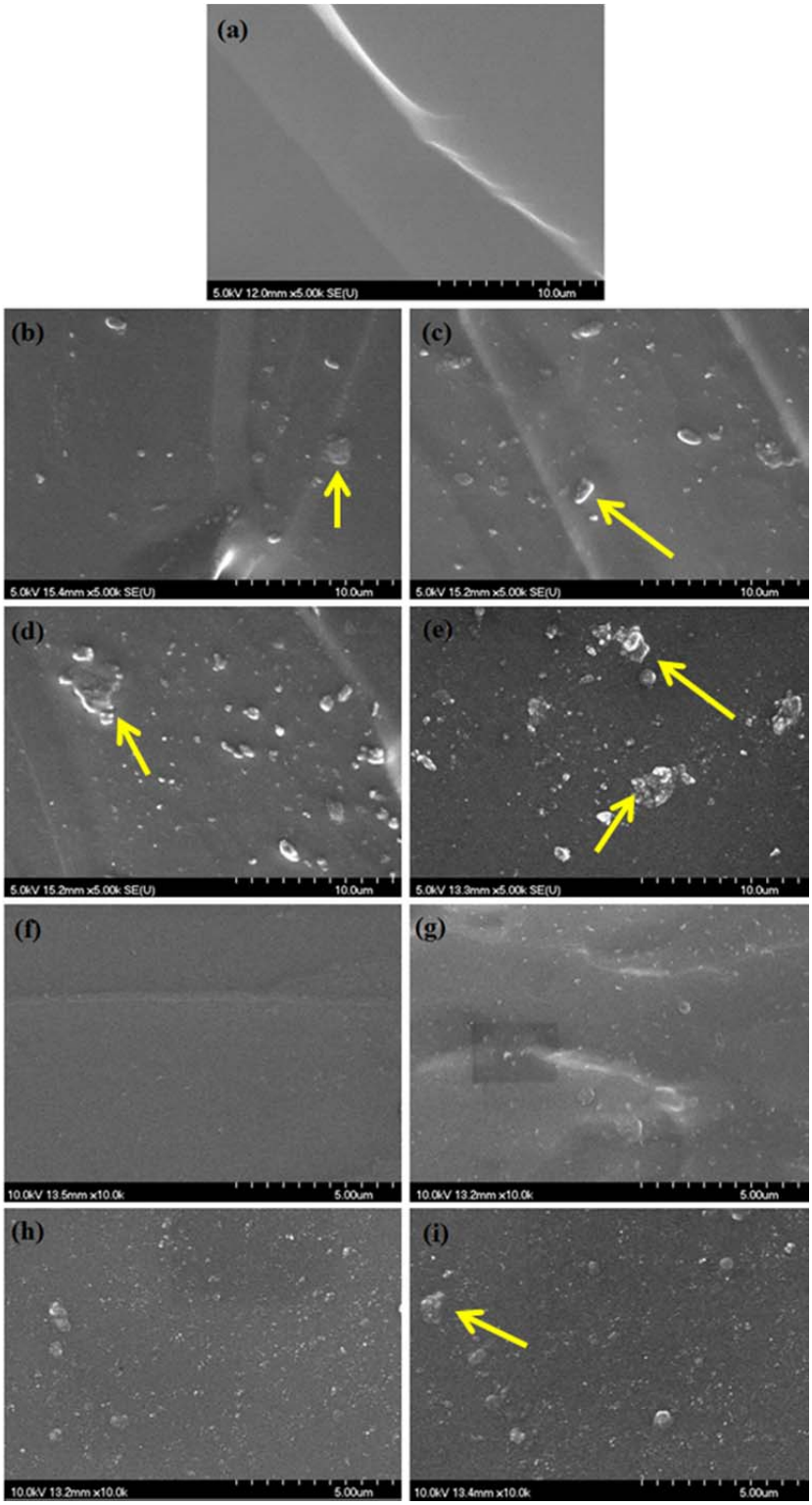

Figure 7. SEM images of the fractured surface of (a) neat SR(b) 0.01 phr pristine TiO_2/SR (×5k), (c) 0.05 phr pristine TiO_2/SR (×5k), (d) 0.10 phr pristine TiO_2/SR (×5k), (e) 0.15 phr pristine TiO_2/SR (×5k), (f) 0.01 phr TMOS-m-TiO_2/SR (×10k), (g) 0.05 phr TMOS-m-TiO_2/SR (×10k), (h) 0.10phr TMOS-m-TiO_2/SR (×10k), and (i) 0.15 phr TMOS-m-TiO_2/SR (×10k).

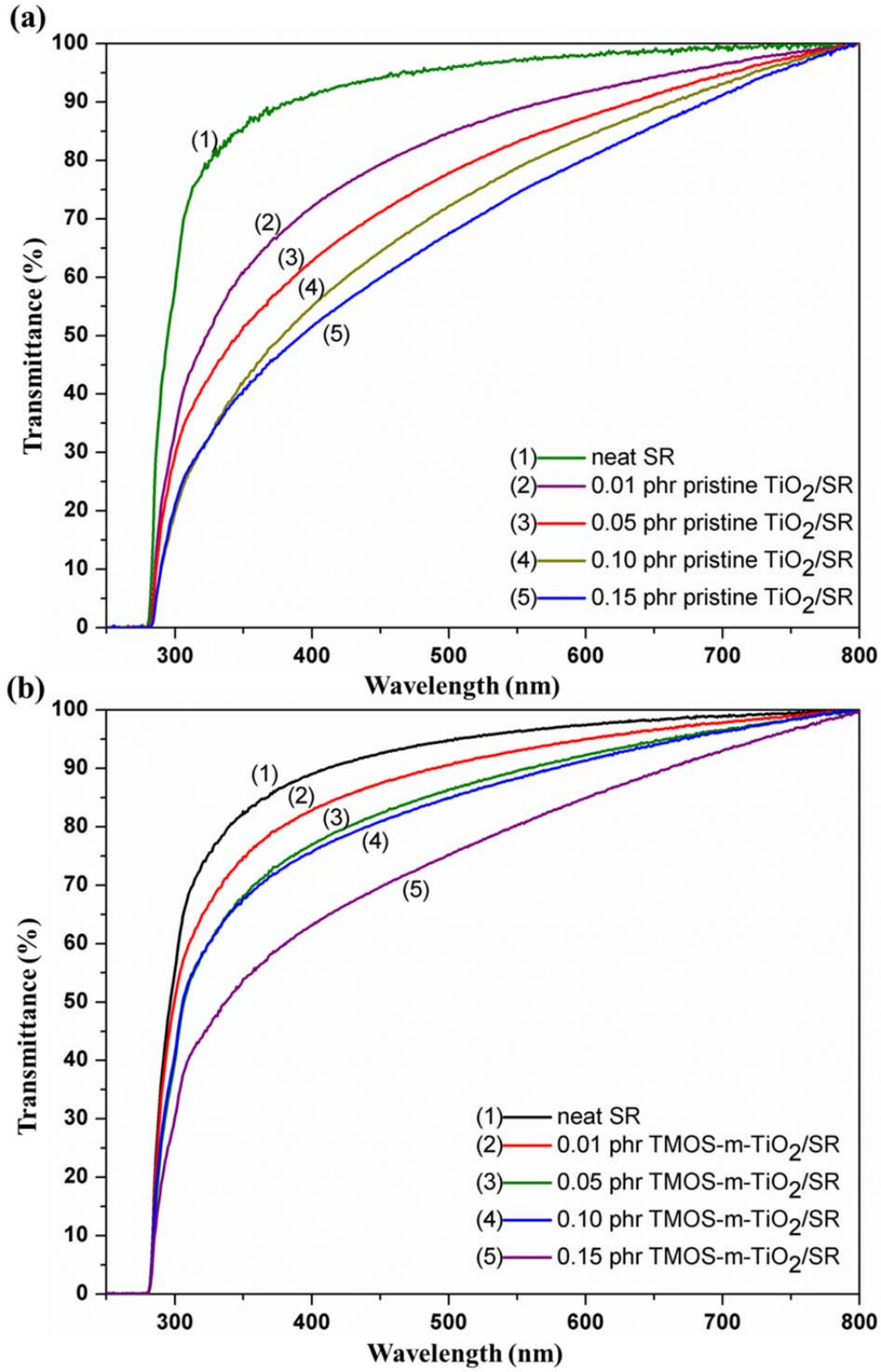

Figure 8. Optical transmittance of (a) pristine TiO_2/SR nanocomposites: (1) neat SR, (2)0.01 phr, (3)0.05 phr, (4)0.10 phr, (5)0.15 phr, and (b)TMOS-m-TiO_2/SR nanocomposites: (1)neat SR, (2)0.01 phr, (3)0.05 phr, (4)0.1 phr, (5)0.15 phr.

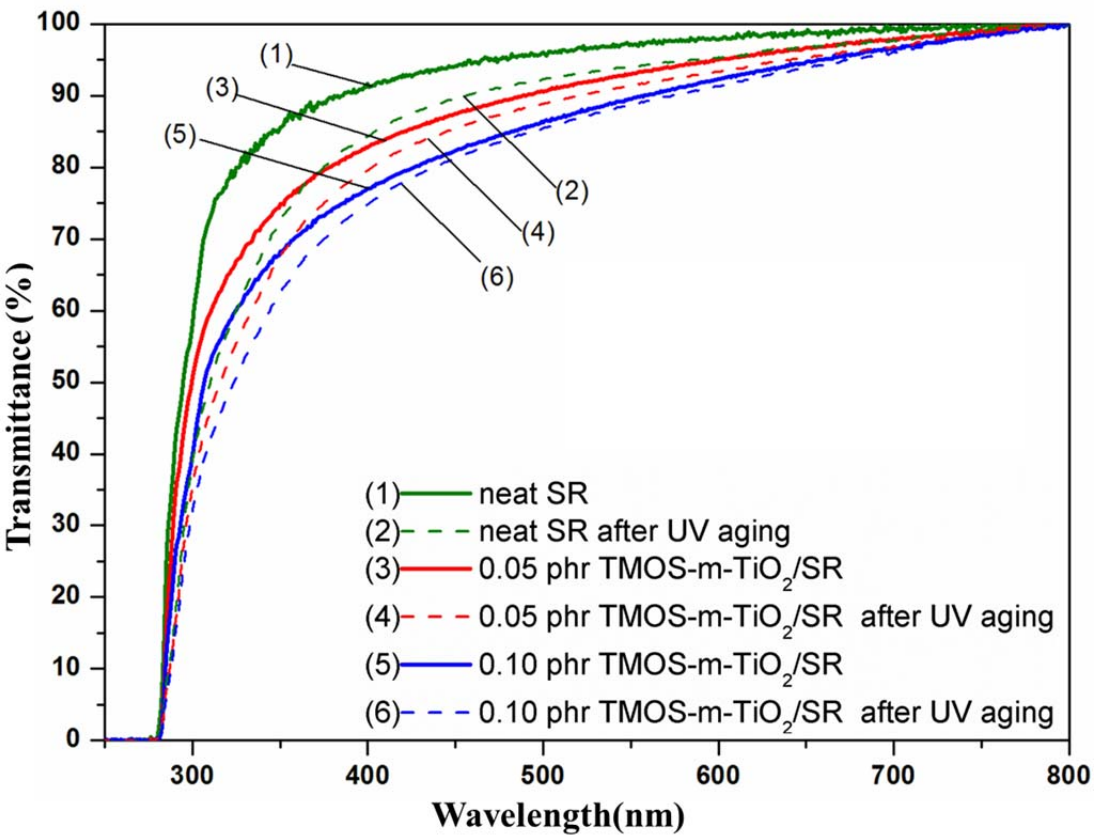

Figure 9. Optical transmittance of TMOS-m-TiO_2/SR composite after UV aging.

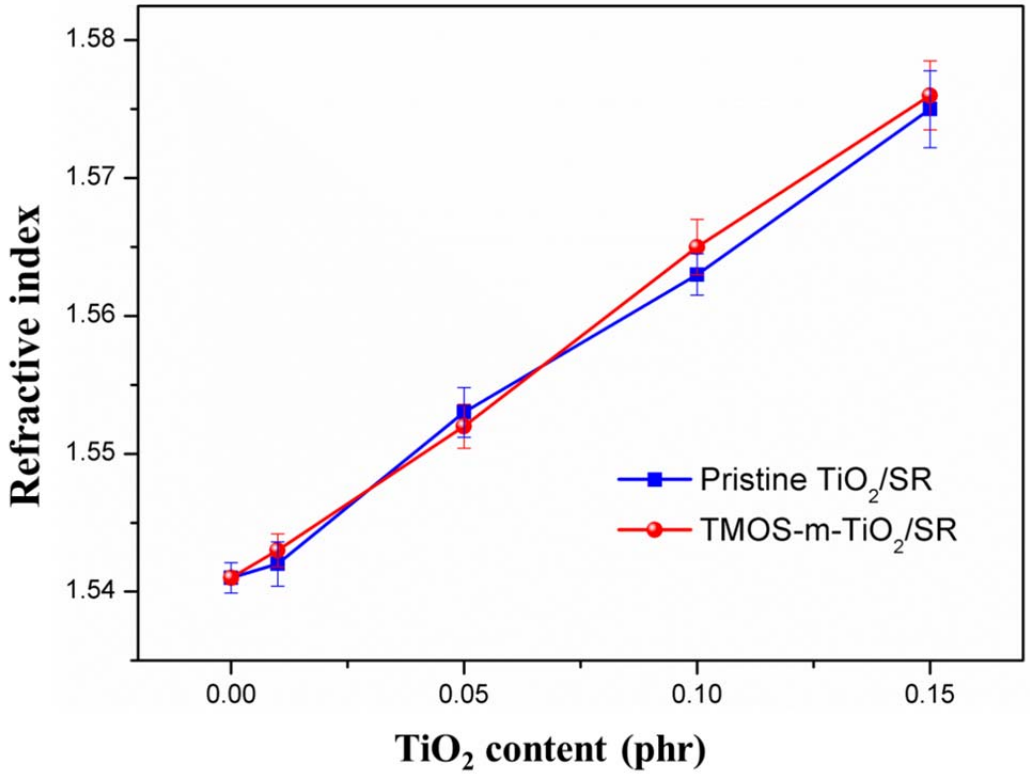

Figure 10. The RI of TiO_2/SR composites with various TiO_2 content.

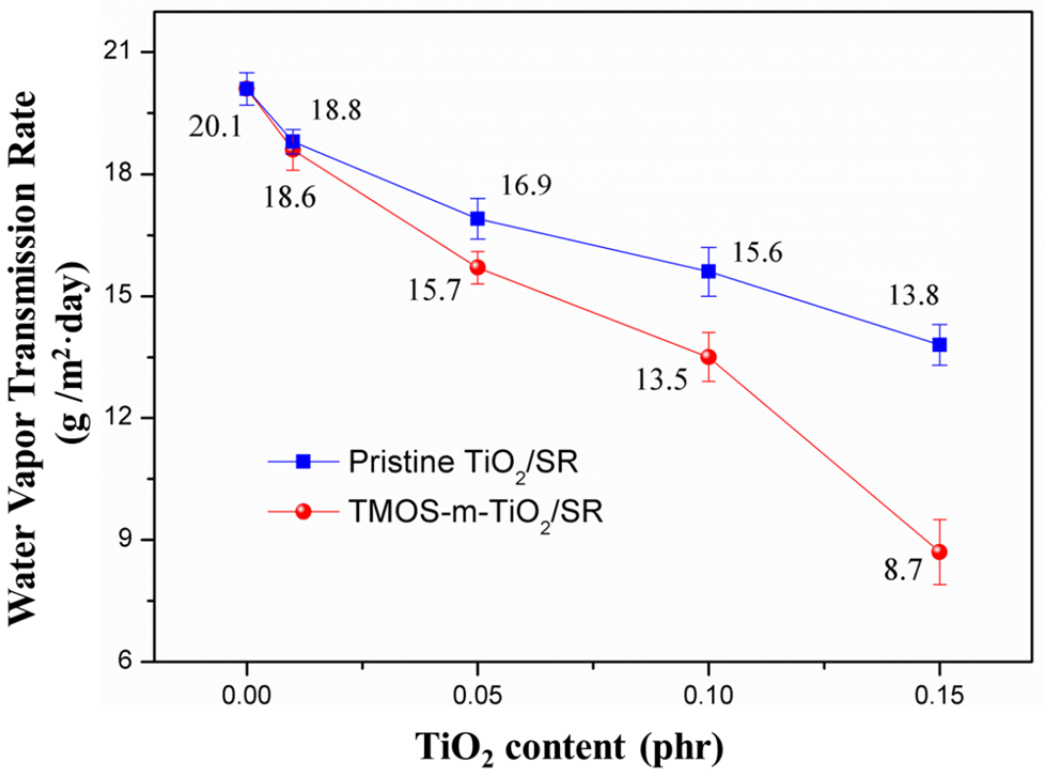

Figure 11. The moisture barrier property of TiO_2/SR composite with various TiO_2 content.

LIST OF TABLES

Table 1

Optical transmittance and transmittance loss after UV aging of TMOS-m-TiO_2/SR composite

Content of TMOS-m-TiO_2 in SR	Transmittance (%) at 450 nm	Transmittance (%) at 450 nm (after UV aging)	Transmittance loss(%)
Neat SR	**94.06±0.55**	**89.69±1.01**	**4.37**
0.01 phr	**92.57±0.62**	**88.63±0.89**	**3.94**
0.05 phr	**87.54±0.76**	**85.53±0.85**	**2.17**
0.10 phr	**82.38±0.78**	**80.97±0.66**	**1.41**